

Ultra-open acoustic metamaterial silencer based on Fano-like interferenceReza Ghaffarivardavagh,¹ Jacob Nikolajczyk,¹ Stephan Anderson,^{2,*} and Xin Zhang^{1,†}¹*Department of Mechanical Engineering, Boston University, Boston, Massachusetts 02215, USA*²*Department of Radiology, Boston University Medical Campus, Boston, Massachusetts 02118, USA*

(Received 18 October 2018; published 4 January 2019)

Recently, with advances in acoustic metamaterial science, the possibility of sound attenuation using subwavelength structures, while maintaining permeability to air, has been demonstrated. However, the ongoing challenge addressed herein is the fact that among such air-permeable structures to date, the open area represents only small fraction of the overall area of the material. In the presented paper in order to address this challenge, we first demonstrate that a transversely placed bilayer medium with large degrees of contrast in the layers' acoustic properties exhibits an asymmetric transmission, similar to the Fano-like interference phenomenon. Next, we utilize this design methodology and propose a deep-subwavelength acoustic metasurface unit cell comprising nearly 60% open area for air passage, while serving as a high-performance selective sound silencer. Finally, the proposed unit-cell performance is validated experimentally, demonstrating a reduction in the transmitted acoustic energy of up to 94%. This ultra-open metamaterial design, leveraging a Fano-like interference, enables high-performance sound silencing in a design featuring a large degree of open area, which may find utility in applications in which highly efficient, air-permeable sound silencers are required, such as smart sound barriers, fan or engine noise reduction, among others.

DOI: [10.1103/PhysRevB.99.024302](https://doi.org/10.1103/PhysRevB.99.024302)**I. INTRODUCTION**

Airborne sound attenuation has conventionally been realized through the application of acoustic barriers by either reflecting or absorbing incident acoustic energy. While wideband attenuation may be obtained, attenuation in the low-frequency regime (< 500 Hz) using such approaches is challenging and necessitates increased acoustic barrier layer thickness. Furthermore and importantly, such methods of sound attenuation eliminate the passage of air, precluding their functionality for applications in which ventilation is required. The need for sound attenuation, while preserving ventilation, such as required in the application to mitigating fan noise, has inspired a range of efforts, often within the context of duct acoustics [1–5]. Among prior efforts, Herschel-Quincke waveguides [6] are notable as narrow-band sound attenuation may be achieved with minimal reduction in the duct air-flow area. Despite the performance of these classical methods for simultaneous sound attenuation and ventilation, their inherent in-duct nature, along with their large physical footprint, have limited their versatility and degree of implementation.

More recently, with ongoing advances in metamaterial science, new possibilities for manipulating acoustic energy have emerged. Metamaterials are composed of subwavelength structures in which their effective acoustic properties are dominated by their structural shape rather than their constitutive materials. Utilizing subwavelength metamaterial structures, phenomena, such as wave-front modulation [7–9], subdiffraction imaging [10,11], and acoustic cloaking [12,13], among

others, have been demonstrated. To date, several acoustic metamaterial-based structures have been proposed to address the challenge of sound attenuation while simultaneously preserving air passage [14–20]. Despite the fact that the reported structures possess a sufficient degree of transmission loss in their designed frequency ranges, the amount of open area of the structures has been sacrificed in order to obtain the desired acoustic performance. Therefore, the ventilation areas of the reported structures are limited to small fractions of the overall area, which, while suitable for air permeability, are problematic in applications of forced ventilation, such as in the case of cooling fans. Recently, Li *et al.* proposed a metamaterial structure composed of a side resonator with the microperforated plates that can absorb the acoustic wave at certain frequencies, while maintaining efficient ventilation [21]. A primary focus of ongoing efforts in this area has been the broadening of the attenuation frequency band, which is substantial in applications of ambient noise reduction, but not requisite in the case of industrial noise, such as machinery or fans, which is harmonic in nature. For instance, in the case of fan noise, the radiated sound is mainly composed of the tonal sound corresponding to the blade-passing frequency and its higher harmonic modes [22,23]. Similarly, in the case of machinery noise, such as engine noise, the radiated sound is mainly composed of higher-order harmonics based on the cylinder firing rate or the engine firing rate [24].

In this paper, we present a design methodology based on Fano-like interference for selective attenuation of the transmitted acoustic wave by means of reflection. The method reported herein enables the design of ultra-open metamaterials (UOM) composed of subwavelength unit-cell structures featuring a predominately open area that provide appropriate functionality when both sound attenuation and highly efficient

*stephan.anderson@bmc.org

†xinz@bu.edu

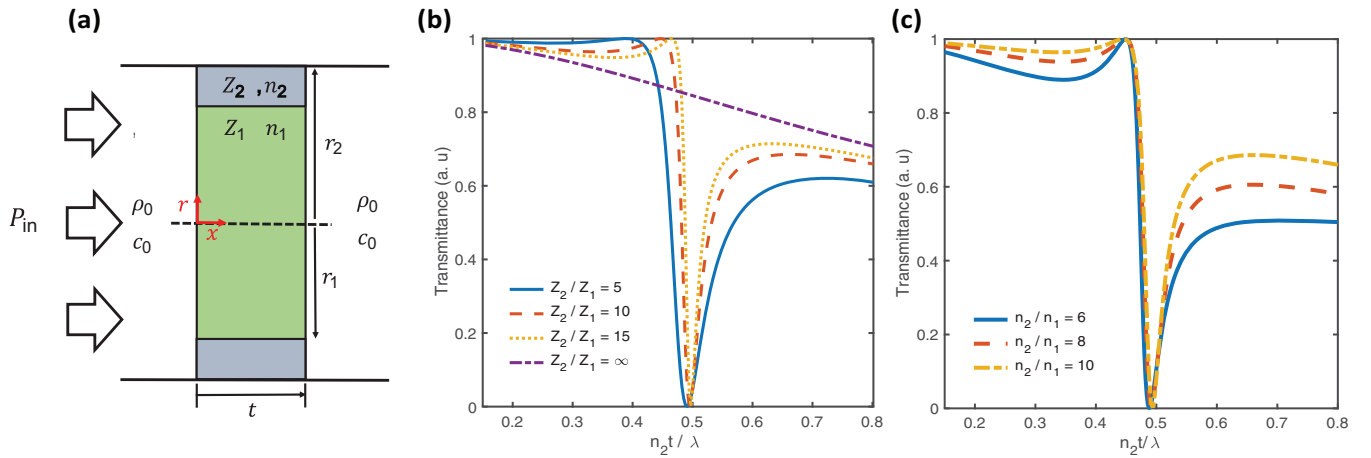


FIG. 1. (a) Transverse bilayer metamaterial. The metamaterial is shown here in which the two colored regions are composed of regions with distinct acoustic properties placed transversely with respect to the wave propagation direction. (b) Acoustic transmittance through the transverse bilayer metamaterial for different values of acoustic impedance contrast (Z_2/Z_1) when the refractive indices ratio is kept constant ($n_2/n_1 = 10$). Notably, for the cases with a finite ratio between the regions' impedance (shown with the blue line, orange dashed line, and the yellow dotted line), Fano-like interference results in a destructive interference. However, in the case of infinite contrast between the regions' impedance, representing orificelike behavior, the destructive interference is suppressed (purple dotted dashed line). (c) Acoustic transmittance through the bilayer metamaterial for different ratios of the refractive indices when the acoustic impedance is kept constant ($Z_2/Z_1 = 10$). For different values of refractive index, destructive interference, i.e., attenuation, occurs where $n_2 t = \lambda/2$ and, consequently, silencing may be realized in the desired frequency regime by tuning the refractive indices.

ventilation are required. Moreover, the presented structures are capable of attenuating the acoustic wave at the targeted frequency as well as its higher harmonics and are therefore readily applicable to attenuate machinery or fan noise. Through the realization of high-performance sound attenuation while retaining air flow, the design methodology enabling UOMs may serve as the foundation of a new generation of acoustic silencing technologies.

II. FANO-LIKE INTERFERENCE IN TRANSVERSE BILAYER METAMATERIALS

Fano was the first to have derived a theory underpinning the asymmetric scattering peaks of electrons during his studies of autoionizing resonance [25]. The origin of the asymmetric scattering profile was explained as a result of the interference between the discrete resonant and continuum states. Recently, given the analogies between physics of phonons and electron scattering [26], the asymmetric scattering of the elastic wave in sonic and phononic crystals based on Fano-like interference is demonstrated [27,28]. This asymmetric transmission profile is due to the fact that the portion of the elastic wave traveling through the resonating element interferes with the portion of the elastic wave traveling through the nonresonating pathway. The asymmetric transmission profile, based on a Fano-like interference possesses a dip region due to destructive interference resulting in attenuation of the transmitted wave. This property of attenuation of the acoustic wave due to Fano-like interference has the potential for applications in acoustic filtering and silencing devices and represents the foundations of the UOM reported herein.

Initially, we aim to analytically demonstrate that such an asymmetric transmission profile based on a Fano-like interference is present in the case of a transverse bilayer metamaterial

shown in Fig. 1. Subsequently, we aim to demonstrate the applicability of the presented metamaterial structure, providing both analytical and experimental validations of a novel acoustic silencing technology.

First, we consider the case of an acoustic plane wave incident on a transverse bilayer metamaterial with distinct acoustic properties as shown in Fig. 1(a). It is assumed herein that the metamaterial has an axisymmetric configuration with respect to the x axis with a thickness of t in which region 1 ($r < r_1$) is composed of a material with acoustic impedance of Z_1 and refractive index of n_1 and region 2 ($r_1 < r < r_2$) is composed of a material with acoustic impedance of Z_2 and refractive index of n_2 . Note that the axisymmetric configuration is selected solely for the purpose of simplification and other configurations may be considered without a loss of generality. Notably, it is assumed herein that two regions are separated with the acoustically rigid spacer at ($r = r_1$) of negligible thickness that eliminates the cross coupling between them. Furthermore, the entire structure is assumed to be confined within a rigid circular waveguide filled with a medium with the sound speed of c_0 and density of ρ_0 for the purposes of deriving the acoustic transmittance.

The transmittance through transverse bilayer metamaterial has been derived analytically using the Green's function theorem (refer to Appendix A for the details of derivation) which has been shown to yield a highly accurate calculation of acoustic transmittance, given its capacity to incorporate the effect of higher-order evanescent modes resulting from an abrupt change in cross section of the wave pathway [29,30]. Using this approach, the transmittance from the bilayer metamaterial for different values of refractive index and acoustic impedance are derived and shown in Figs. 1(b) and 1(c). In Fig. 1(b), it is considered that $n_2/n_1 = 10$ and the transmittance is depicted as a function of the nondimensional quantity

$n_2 t / \lambda$ (λ denotes the wavelength) for four different values of the impedance ratio. In Fig. 1(c), the impedance ratio has been kept constant ($Z_2/Z_1 = 10$), and the transmittance is depicted for three different values of the refractive index ratio. Notably, the background medium within the waveguide is considered to be air, and it is assumed that the medium in region 1 is identical to the background medium. Hence, the acoustic impedance of region 1 may be derived as $Z_1 = \rho_0 c_0 / \pi r_1^2$, and the refractive index (n_1) is equal to unity. From the resulted transmittance curve, it may be observed that, for different values of Z_2 and n_2 , given the differing acoustic properties of regions 1 and 2, an asymmetric transmission profile is obtained in which destructive interference may result in zero transmittance due to Fano-like interference. The destructive interference emerges where $n_2 t = \lambda/2$, which is the resonating state of region 2. Given the contrast in refractive indices of the two regions, region 1 remains in a continuum state and, consequently, a Fano-like interference occurs. During this state, the portion of the acoustic wave traveling through region 2 interacts with resonance-induced localized modes in this region, resulting in an out-of-phase condition after traveling through region 2. The portion of the incident acoustic wave traveling through region 1 will pass the metamaterial with negligible phase shift and, consequently, a resultant destructive interference occurs on the transmission side of the metamaterial.

By comparing the transmittance for different values of the impedance ratio, it may be inferred that by increasing the contrast between the acoustic impedances of the two regions, the quality factor (Q factor) of the attenuation performance is increased. This attribute provides a degree of freedom through which, by adjusting the impedance contrast, the proper frequency bandwidth may be realized. Notably, when the acoustic impedance ratio yields a very large number ($Z_2/Z_1 = \infty$), the filtration performance is suppressed, given its marked narrow-band character, and an orificelike behavior is realized. However, an orifice structure with a similar open area geometry results in a relatively poor sound filtration performance, leading to only minor degrees of attenuation of the transmitted acoustic wave. Figure 1(c), demonstrates the effect of refractive index contrast between the two media on transmittance and illustrates that high degrees of filtration are obtained when $n_2 t = \lambda/2$. Thus, by adjusting the refractive indices in the proposed structure, high-performance sound attenuation may be realized at any desired frequency.

Of note, the destructive interference initially occurs at $n_2 t = \lambda/2$, which is the first resonance mode of region 2 but will also occur at higher resonance modes when $n_2 t = N\lambda/2$ for integers of N shown in Fig. 2(a). To this end, the silencing behavior of the transverse bilayer metamaterial has been investigated for the case of a normally incident acoustic plane wave. However, given the subwavelength nature of the proposed metamaterial structure, it is expected that silencing will be also present in the case of oblique incidence. To validate this expectation, full-wave simulation was utilized, and the transmittance through the transverse bilayer metamaterial in the case of oblique incidence with different incident angles was derived and shown in Fig. 2(b). From Fig. 2(b), it can be observed that the silencing functionality of the proposed

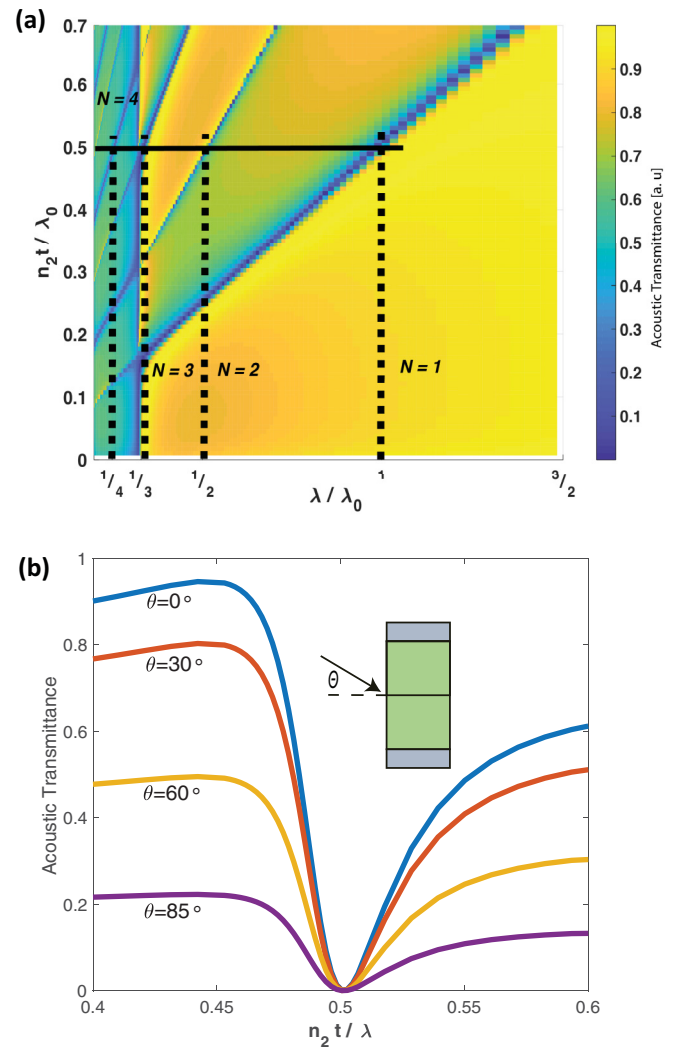


FIG. 2. (a) Acoustic transmittance from transverse bilayer metamaterial structure with different refractive index ratios and a constant impedance ratio of ten. The silencing functionality initially emerges when $n_2 t = \lambda/2$ but is also present in higher-order harmonics when $n_2 t = N\lambda/2$. (b) Acoustic transmittance through the transverse bilayer metamaterial in the case of oblique incidence with different incident angles.

metamaterial structure is present even for very large angles of incidence.

The methodology presented herein and based on a Fano-like interference in a bilayer metamaterial structure offers a design platform to selectively silence unwanted sound. Using this design, by tuning the acoustic impedance and refractive index contrast between the two regions of the metamaterial, the desired acoustic filtration performance may be achieved. In the following sections, we utilize this concept to design a metamaterial structure that features a large open area for air transport while also selectively silencing unwanted sound.

III. UOM FOR SELECTIVE SOUND SILENCING

In this section, a UOM structure based on the concept of the bilayer metamaterial is designed, and its performance in sound silencing experimentally validated. The UOM structure

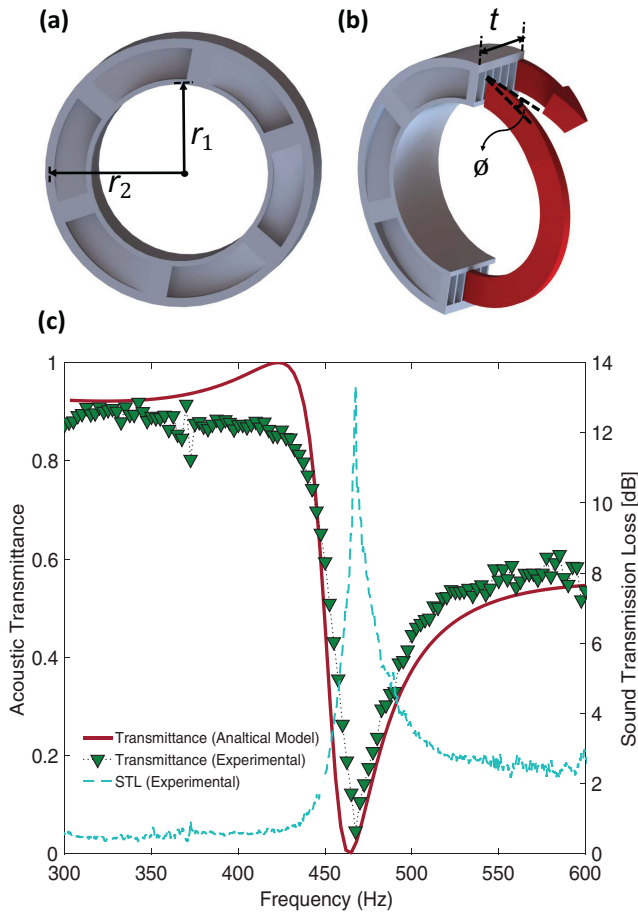


FIG. 3. (a) UOM structure is shown in which the open region at the center ($r < r_1$) corresponds to region 1 in the transverse bilayer metamaterial and the outer region, featuring six channels coiled in the form of helix ($r_1 < r < r_2$), corresponds to region 2. (b) Internal structure of the UOM is shown with an acoustic wave traveling through the channels and essentially following the helical pathway with a helix angle of ϕ . (c) Acoustic transmittance resulting from the impedance tube experiment is shown with the dotted-line with a triangular marker demonstrating that near 460 Hz, the transmittance is reduced to the minimum value of approximately 0.06. Sound transmission loss (STL) for the wave passing through the UOM is also shown with the dashed line corresponding the rightward y-axis. The solid line represents the predicted behavior using the Green's function method by modeling the UOM structure as a transverse bilayer metamaterial.

is shown in Fig. 3(a), the effective acoustic model of which may be simplified to the form of the transverse bilayer metamaterial structure. The center portion of the designed structure ($r < r_1$) is completely open area which yields a high degree of air transport. This region corresponds to region 1 in the bilayer metamaterial structure, and its acoustic impedance may be derived as $\rho_0 c_0 / \pi r_1^2$ where ρ_0 and c_0 are the density and sound speed of the background medium, respectively. Notably, the acoustic refractive index of this region is equal to unity. As discussed above, in order to obtain the desired silencing functionality, a contrast in the acoustic properties of two regions is essential. The difference in acoustic properties of the two regions may provide the resonating state condition in region

2, whereas region 1 remains in the continuum state. Therefore, in order to realize the contrast in the acoustic properties of the two regions, the concept of a helical metamaterial structure is utilized herein. Helical metamaterials are founded on the basis of space-coiling metamaterials in which the acoustic wave pathway represents the form of a helix. In these structures, by tailoring the geometrical parameters, the desired effective refractive index and effective acoustic impedance may be obtained and their application in wave-front manipulation has been demonstrated [31,32]. In the helical metamaterial regime ($r_1 < r < r_2$), which corresponds to region 2 in the transverse bilayer metamaterial, six air channels are coiled in the form of a helix in which the extended path length of the acoustic wave provides a large effective refractive index in this region. Moreover, the small cross-sectional area of the helix channels in comparison to the waveguide yields a large acoustic impedance in this region. The internal features of the UOM are shown in Fig. 3(b) in which the red arrow illustrates the pathway through the helical channels.

The acoustic impedance of the helical region may be approximated as $\rho_0 c_0 / t(r_2 - r_1)$ in which t , r_1 , and r_2 are structure thickness, inner radius, and outer radius, respectively, and which are shown in Fig. 3(a). The contrast or ratio between the acoustic impedances of the two regions may be expressed as

$$Z_2/Z_1 = \pi r_1^2 / t(r_2 - r_1). \quad (1)$$

Considering the effective path length of the acoustic wave traveling through the helical channels, the effective refractive index of the helical region may be approximated as [31]

$$n_2 = 1 / \sin(\phi), \quad (2)$$

where ϕ denotes the helix angle shown in Fig. 3(b). From Eqs. (1) and (2), it can be inferred that by adjusting the helix angle (ϕ), the desired refractive index, and the values of the t , r_1 , and r_2 parameters, the desired impedance ratio may be realized. Noteworthy is the fact that the presented design offers a number of highly valuable degrees of freedom to optimize device performance and tailor applicability. The refractive index as is expressed in Eq. (2) depends solely on the helix angle, which may be independently tailored without any effect on other design parameters. In addition, the acoustic impedance ratio derived in Eq. (1) is a function of three geometrical parameters for which there exist infinite sets of values leading to any desired relative impedance value. Therefore, based on design preference, such as a preference for thinning the structure (small value of t) or increasing the open area of the structure (increasing r_1/r_2), an optimal metamaterial unit-cell structure may be readily designed.

Finally, in order to experimentally validate the performance of the UOM structure, a UOM has been designed with the aim of silencing sound with a frequency near 460 Hz and, therefore, was fabricated with dimensions of $t = 5.2$, $r_1 = 5.1$, $r_2 = 7$ cm, and $\phi = 8.2^\circ$. Please note that the overall size of the fabricated UOM herein is deep subwavelength in nature and, for instance, the UOM's thickness approximates 0.07λ whereas λ at 460 Hz approximates 74.5 cm. Employing Eqs. (1) and (2), the UOM may be simply modeled as a transverse bilayer metamaterial with an acoustic impedance ratio

of $Z_2/Z_1 = 7.5$ and refractive index ratio of $n_2/n_1 = 7$, approximated based on the fabricated UOM dimensions. Please note that the assumption with regard to the presence of an acoustically rigid spacer utilized in the analysis of the case of the transverse bilayer metamaterial is also relevant for the proposed UOM silencer. The two regions of the fabricated UOM structure are separated with an acrylonitrile butadiene styrene (ABS) plastic layer of 6 mm that results in approximately 29-dB transmission loss at 450 Hz for the wave traveling from the open region of the UOM to the helical metamaterial region and vice versa. Based on this large transmission loss expected from this layer, the interface between the two regions may be reasonably approximated as a rigid spacer layer, such as was assumed in transverse bilayer metamaterial structure. Consequently, the equivalent model of the presented UOM structure may be simplified to the form of the transverse bilayer metamaterial discussed in the previous section.

The fabricated UOM structure was experimentally tested using an air-filled impedance tube with the transmittance derived in the frequency range of 300–600 Hz (Refer to the Appendix B for detail of Fabrication and Experiment). The experimental result is shown in Fig. 3(c) in which the transmittance (leftward y axis) is shown with a dotted line with a triangular marker and its representation in sound transmission loss (STL) (rightward y axis) is shown with the dashed line. Additionally, based on the transverse bilayer metamaterial model and using the effective acoustic properties estimated for the fabricated UOM, transmittance has been derived analytically and is shown in Fig. 3(c) (solid line). As demonstrated in Fig. 3(c), the experimentally measured transmittance through

the UOM structure exhibits an asymmetric profile possessing a dip region where destructive interference due to Fano-like interference has silenced the transmitted wave. Notably, the experimental results obtained herein are in agreement with the predicted analytical solution and, consequently, the applicability of the analytical model for the design of this class of metamaterial structures is validated. Based on our experimental results, the transmitted acoustic energy is decreased to approximately 6% at the peak frequency, indicating that approximately 94% of the acoustic wave energy is blocked using the proposed structure. Moreover, there exists a high degree of agreement between the peak filtration frequency band when comparing the analytical and experimental results and the fact that that the experimentally obtained peak frequency is in close proximity to the regime where $n_2t = \lambda/2$ is readily confirmed. Please note that due to limitations in the fabrication precision of the metamaterial structure, the targeted frequency in the UOM design step has been selected to approximate 460 Hz, although device performance may readily be realized at lower frequencies simply by decreasing the helix angle.

Furthermore, in order to visualize the silencing performance of the UOM structure and gain a deeper insight into its performance, the sound transmission through the UOM is modeled numerically using COMSOL finite element software. Given the complexity associated with the helical shape of the UOM’s channel, sound transmission has been modeled in three-dimensional (3D) space, but a cut plane is used to demonstrate the resultant pressure and velocity fields in two dimensions (2D), shown in Figs. 4(a) and 4(b). The

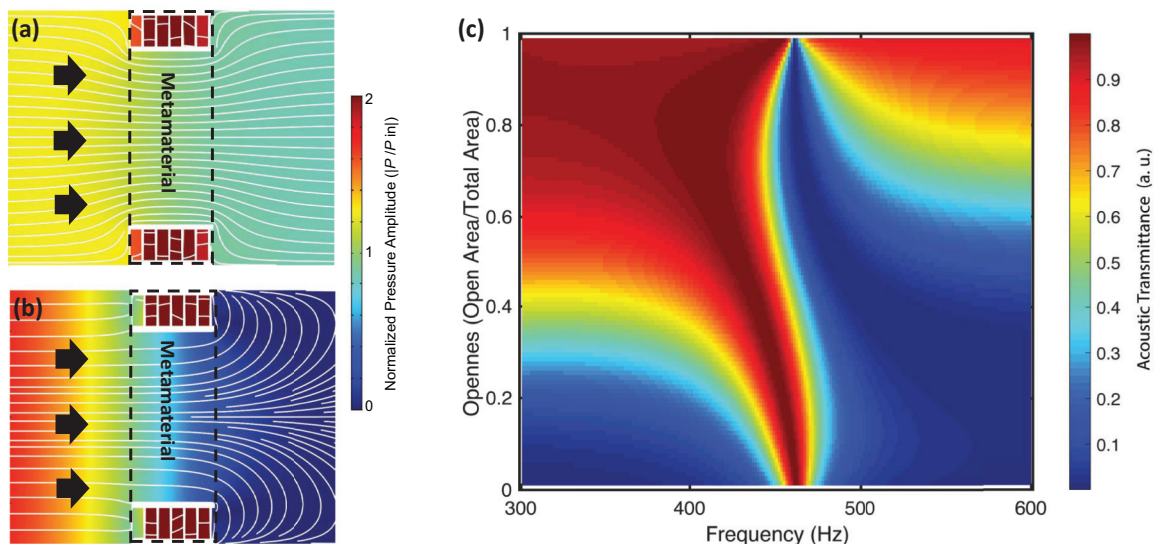


FIG. 4. (a) The absolute pressure value normalized by the incident wave magnitude resulting from a plane wave with a frequency of 400 Hz and incident on the UOM from the left-hand side is shown using a color map. The local velocity stream is shown with the white lines. At this frequency, the transmission coefficient is about 0.85, hence, approximately 72% of the acoustic wave energy is transmitted. (b) The pressure and velocity profile is depicted with an incident plane wave of the same amplitude but a frequency of 460 Hz. At this frequency, due to Fano-like interference, the transmitted wave has a markedly decreased amplitude, and the wave has been silenced. In this case, the phase difference between the transmitted waves from the two regions of the metamaterial has resulted in a curvature of the wave velocity field and has diminished the far-field radiation. (c) Acoustic transmittance through UOM structures with different degrees of structure openness. Transmittance has been analytically derived using the Green’s function method. Notably, UOM structures considered herein feature identical refractive index ratios in their transverse bilayer metamaterial model but have different impedance ratios.

background color represents the absolute value of the pressure field normalized by the amplitude of the incident wave, and the white lines reflect the stream and orientation of the local velocity field. Demonstrated in Fig. 4(a) is a plane wave with frequency of 400 Hz incident on the metamaterial from the left side as shown with black arrows. In accordance with the analytically and experimentally expected behaviors of the UOM structure, in the frequency regime of 400 Hz, high-pressure transmission results. At this state, given the fact that the helical portion of the UOM structure possesses a markedly larger acoustic impedance in comparison with the open portion in the center, the incident wave will predominately travel through the central open portion of the UOM. This behavior may be visually confirmed with the local velocity field stream shown in Fig. 4(a) where both preceding and beyond the UOM structure, the velocity field exhibits minimal disturbance save for the change in cross-sectional area. In Fig. 4(b), a similar case of a plane wave incident from the left side is demonstrated but with a frequency of 460 Hz. Based on the theoretical and experimental results obtained above, it is expected that at this frequency, the wave transmitted through the helical portion of the UOM will become out of phase with the transmitted wave traveling through the central open portion of the metamaterial. The results obtained herein confirm this expectation, demonstrating that the destructive interference on the transmission side (right side) of the UOM has resulted in effectively eliminating wave transmission. Notably, the out-of-phase transmission through the two regions of the UOM may be further validated using the velocity profile shown in Fig. 4(b) with white lines. It may be readily observed that the local acoustic velocities of the transmitted wave from the two regions of the UOM are in opposite directions, resulting in a marked curvature of the velocity stream and diminished far-field radiation. It should be mentioned that, with the presence of the destructive interference due to Fano-like interference, the metamaterial structure mimics the case of an open-end acoustic termination in which near-zero effective acoustic impedance results in a predominant reflection of the incident wave.

The UOM structure experimentally validated herein features a nearly 60% open area, which yields the capacity for both efficient ventilation in combination with high-performance selective sound silencing. Importantly, the presented methodology based on the transverse bilayer metamaterial concept and employed to design the UOM structure does not impose any inherent limitation on the area fraction of the central open region. As shown in Fig. 1(b) with an increase in the ratio between the acoustic impedance of two regions, silencing functionality will be achieved, although in a narrower band of frequency. Considering the fact that openness percentage may be very well correlated with the acoustic impedance ratio, it is expected that even with very high openness percentage, silencing can be realized within the scope of the presented methodology. This assumption has been validated by analytically retrieving the acoustic transmittance through the UOM structure with different openness values, shown in Fig. 4(c). It may be observed that even for

UOM structures with a very high percentage of open area (approaching nearly complete open area where openness approximates 1), the silencing functionality remains present with a resultant decreased in the silenced frequency bandwidth.

Notably, in the present paper, the structural elements of the proposed UOM have been considered acoustically rigid in both analytical and numerical approaches. The rigidity assumption employed herein is supported by the fact that the ABS layers of the fabricated UOM structures result in a transmission loss in the targeted frequency range of a magnitude such that these layers may be safely considered as rigid. However, when targeting the silencing the very low frequency or when the UOM is employed as a building block of a larger element, such as a silencer wall, the acoustic structure interaction needs to be considered and may not simply be omitted.

IV. CONCLUSION

In the paper presented herein, we have introduced a metamaterial-based design methodology for air-permeable sound silencing. First, inspired by the Fano-like interference phenomena, a transverse bilayer metamaterial concept is proposed from which destructive interference may be employed for acoustic silencing. Next, a UOM structure was designed accordingly and experimentally validated. The designed metamaterial possesses two distinguishable regions, the central open portion and the peripheral helical portion with a contrast in their acoustic properties. The central open portion of the metamaterial provides a large degree of open area for air transport. Importantly, the design of the proposed metamaterial is inherently flexible as discussed above. Therefore, based on the required degree of ventilation for a particular application, the open central of the UOM metamaterial may readily be expanded to meet any ventilation requirement while maintaining acoustic wave silencing functionality.

The metamaterial-based methodology for the design of an air-permeable acoustic silencer presented herein provides an effective and versatile tool for the design of next generation acoustic silencing devices. Utilizing this method, subwavelength and lightweight structures featuring high degrees of open area may be designed to silence specific frequency bands of unwanted sound along with their higher modes.

ACKNOWLEDGMENTS

We would like to sincerely thank Prof. R. G. Holt for the fruitful discussion. The authors would like to acknowledge Boston University Materials Innovation Grant and the Dean's Catalyst Award. The authors also thank the Boston University Photonics Center for technical support. R.G., S.A., and X.Z. conceived the idea and interpreted the results. R.G. designed and performed the theoretical and numerical calculations. J.N. helped with the numerical simulations. R.G. and J.N. designed and performed the experiment. R.G., S.A., and X.Z. contributed to the preparation and writing of the paper, and X.Z. planned, coordinated, and supervised the project.

APPENDIX A: ANALYTICAL DERIVATION OF ACOUSTIC TRANSMITTANCE FROM TRANSVERSE BILAYER METAMATERIAL USING THE GREEN'S FUNCTION METHOD

In the transverse bilayer metamaterial, given its inherent transverse nature, both pressure and velocity field at the boundaries of the metamaterial will be a function of r . Hence, as the first step to derive the transmittance, the following definitions of acoustic pressure and velocity field at the interfaces ($x = 0$ and $x = t$) are employed to relieve the transverse variation of the pressure and velocity fields,

$$\overline{P}_1(x = 0) = \frac{2\pi}{\pi r_1^2} \int_0^{r_1} p(r, x) \Big|_{x=0} r dr, \quad (\text{A1})$$

$$\overline{P}_2(x = 0) = \frac{2\pi}{\pi(r_2^2 - r_1^2)} \int_{r_1}^{r_2} p(r, x) \Big|_{x=0} r dr, \quad (\text{A2})$$

$$\overline{P}_1(x = t) = \frac{2\pi}{\pi r_1^2} \int_0^{r_1} p(r, x) \Big|_{x=t} r dr, \quad (\text{A3})$$

$$\overline{P}_2(x = t) = \frac{2\pi}{\pi(r_2^2 - r_1^2)} \int_{r_1}^{r_2} p(r, x) \Big|_{x=t} r dr, \quad (\text{A4})$$

$$\overline{U}_1(x = 0) = 2\pi \int_0^{r_1} u(r, x) \Big|_{x=0} r dr, \quad (\text{A5})$$

$$\overline{U}_2(x = 0) = 2\pi \int_{r_1}^{r_2} u(r, x) \Big|_{x=0} r dr, \quad (\text{A6})$$

$$\overline{U}_1(x = t) = 2\pi \int_0^{r_1} u(r, x) \Big|_{x=t} r dr \quad (\text{A7})$$

$$\overline{U}_2(x = t) = 2\pi \int_{r_1}^{r_2} u(r, x) \Big|_{x=t} r dr, \quad (\text{A8})$$

in which p and u are acoustic pressure and the velocity field, respectively. $\overline{P}_{1,2}$ and $\overline{U}_{1,2}$ are the averaged pressure and volume velocity at region 1 and region 2 interfaces with the medium inside the waveguide.

Next, considering that the regions are separated with a hard boundary, the propagation of the acoustic wave within each region may be considered independently. Consequently, the transfer matrices relating the output pressure, and velocity to the input conditions for regions 1 and 2 may be written in a decoupled fashion. Considering the case of plane-wave propagation, the transfer matrices of these regions may be derived as follows:

Acoustic pressure and velocity in these regions following the $-i\omega t$ convention may be written as

$$\overline{P}_m(x) = A_1 e^{ik_0 n_m x} + A_2 e^{-ik_0 n_m x}, \quad (\text{A9})$$

$$\overline{U}_m(x) = \frac{A_1 e^{ik_0 n_m x}}{Z_m} - \frac{A_2 e^{-ik_0 n_m x}}{Z_m}, \quad (\text{A10})$$

in which k_0 is the wave number associated with the medium within the duct, defined as $k_0 = \frac{\omega}{c_0}$, n_m and Z_m are the effective refractive index and effective acoustic impedance of region m , respectively. A_1 and A_2 are constant coefficients associated with the outgoing and incoming waves, respectively. Employing Eqs. (A9) and (A10), the averaged pressure and volume velocity at $x = 0$ and $x = t$ may be derived as

$$\overline{P}_m(x = 0) = A_1 + A_2, \quad (\text{A11})$$

$$\overline{U}_m(x = 0) = \frac{A_1}{Z_m} - \frac{A_2}{Z_m}, \quad (\text{A12})$$

$$\overline{P}_m(x = t) = A_1 e^{ik_0 n_m t} + A_2 e^{-ik_0 n_m t}, \quad (\text{A13})$$

$$\overline{U}_m(x = t) = \frac{A_1 e^{ik_0 n_m t}}{Z_m} - \frac{A_2 e^{-ik_0 n_m t}}{Z_m}. \quad (\text{A14})$$

By first deriving A_1 and A_2 in terms of $\overline{P}_m(x=0)$ and $\overline{U}_m(x=0)$ using Eqs. (A11) and (A12) and then substituting them into Eqs. (A13) and (A14), one may find the transfer matrices for regions 1 and 2 ($m = 1, 2$) as

$$\begin{bmatrix} \overline{P}_1(x=0) \\ \overline{U}_1(x=0) \end{bmatrix} = \begin{bmatrix} \cos(k_0 n_1 t) & -i Z_1 \sin(k_0 n_1 t) \\ -\frac{i}{Z_1} \sin(k_0 n_1 t) & \cos(k_0 n_1 t) \end{bmatrix} \begin{bmatrix} \overline{P}_1(x=t) \\ \overline{U}_1(x=t) \end{bmatrix} \quad (\text{A15})$$

$$\begin{bmatrix} \overline{P}_2(x=0) \\ \overline{U}_2(x=0) \end{bmatrix} = \begin{bmatrix} \cos(k_0 n_2 t) & -i Z_2 \sin(k_0 n_2 t) \\ -\frac{i}{Z_2} \sin(k_0 n_2 t) & \cos(k_0 n_2 t) \end{bmatrix} \begin{bmatrix} \overline{P}_2(x=t) \\ \overline{U}_2(x=t) \end{bmatrix}. \quad (\text{A16})$$

To this end, the relation between the input pressure and the velocity to the output condition within each region of the metamaterial has been derived in terms of the transfer matrices. The next step in deriving the transmittance is to investigate the interaction between the acoustic wave inside the duct and the transverse bilayer metamaterial's interfaces at $x = 0$ and $x = t$. In order to investigate this interaction, the Green's function method is utilized herein, which is essentially the response of the system to the point source. Utilizing the Green's function and given the fact that any source distribution may be written as an integral of the point sources, one may readily derive the resultant acoustic field.

Green's function $G(r, x; r_0, x_0)$ within a semi-infinite circular duct terminating at $x = 0$ may be derived as the solution of the Helmholtz equation [29],

$$\nabla^2 G(r, x; r_0, x_0) + k_0^2 G(r, x; r_0, x_0) = -\frac{\delta(r-r_0)\delta(x-x_0)}{2\pi r}, \quad (\text{A17})$$

where δ represents the Dirac function. From the solution of Eq. (A11), the Green's function with respect to the incident and transmitted side of the metamaterial can be obtained as [30]

$$x \leq 0: G_1(r, x; r_0, x_0) = \sum_{n=0}^{\infty} \frac{\varphi_n(r_0)\varphi_n(r)}{-2i\pi r_0^2 \sqrt{k_0^2 - k_n^2}} \left(e^{i\sqrt{k_0^2 - k_n^2}|x-x_0|} + e^{i\sqrt{k_0^2 - k_n^2}|x+x_0|} \right), \quad (\text{A18})$$

$$x \geq t: G_2(r, x; r_0, x_0) = \sum_{n=0}^{\infty} \frac{\varphi_n(r_0)\varphi_n(r)}{-2i\pi r_0^2 \sqrt{k_0^2 - k_n^2}} \left(e^{i\sqrt{k_0^2 - k_n^2}|x-x_0|} + e^{i\sqrt{k_0^2 - k_n^2}|x+x_0-2t|} \right). \quad (\text{A19})$$

When r_2 and t are the duct radius and metamaterial's thickness, respectively, as shown in Fig. 1 and the eigenmode is defined as $\varphi_n(r) = J_0(k_n r)/J_0(k_n r_2)$ with the wave-number k_n as the solution of $J'(k_n r_2) = 0$ when J represents the Bessel function.

Utilizing the Kirchhoff-Helmholtz integral, the pressure field on the left side of the metamaterial ($x \leq 0$) may be written as [29]

$$p(r, x) = e^{ik_0 x} + e^{-ik_0 x} + 2\pi \int_0^{r_1} G_1(r, x; r_0, x_0) \frac{\partial p(r_0, x_0)}{\partial x_0} \Big|_{x_0=0} r_0 dr_0 + 2\pi \int_{r_1}^{r_2} G_1(r, x; r_0, x_0) \frac{\partial p(r_0, x_0)}{\partial x_0} \Big|_{x_0=0} r_0 dr_0. \quad (\text{A20})$$

By applying the conservation of the momentum, one may write

$$i\omega\rho_0 u(r, 0) = -\frac{\partial p(r_0, x_0)}{\partial x_0} \Big|_{x_0=0}. \quad (\text{A21})$$

By first rewriting the pressure gradient term in Eq. (A20) using Eq. (A21), and subsequently employing Eqs. (A5) and (A6), one may derive

$$p(r, 0) = 2 + 2\pi i\omega\rho_0 \frac{\overline{U}_1(x=0)}{\pi r_1^2} \int_0^{r_1} G_1(r, 0; r_0, 0) r_0 dr_0 + 2\pi i\omega\rho_0 \frac{\overline{U}_2(x=0)}{\pi(r_2^2 - r_1^2)} \int_{r_1}^{r_2} G_1(r, 0; r_0, 0) r_0 dr_0. \quad (\text{A22})$$

By substituting the $p(r, 0)$ found from Eq. (A22) into Eqs. (A1) and (A2), one may readily derive that

$$\overline{P}_1(x=0) = 2 + \frac{4i\rho_0\omega\overline{U}_1(x=0)}{r_1^4} \int_0^{r_1} \int_0^{r_1} G_1(r, 0; r_0, 0) r_0 dr_0 r dr + \frac{4i\rho_0\omega\overline{U}_2(x=0)}{r_1^2(r_2^2 - r_1^2)} \int_0^{r_1} \int_{r_1}^{r_2} G_1(r, 0; r_0, 0) r_0 dr_0 r dr, \quad (\text{A23})$$

$$\overline{P}_2(x=0) = 2 + \frac{4i\rho_0\omega\overline{U}_1(x=0)}{r_1^2(r_2^2 - r_1^2)} \int_{r_1}^{r_2} \int_0^{r_1} G_1(r, 0; r_0, 0) r_0 dr_0 r dr + \frac{4i\rho_0\omega\overline{U}_2(x=0)}{(r_2^2 - r_1^2)^2} \int_{r_1}^{r_2} \int_{r_1}^{r_2} G_1(r, 0; r_0, 0) r_0 dr_0 r dr. \quad (\text{A24})$$

Similarly, when $x \geq t$, following the same procedure and employing the Green's function $G_2(r, x; r_0, x_0)$, the pressure may be derived as

$$\overline{P}_1(x = t) = -\frac{4i\rho_0\omega\overline{U}_1(x = t)}{r_1^4} \int_0^{r_1} \int_0^{r_1} G_2(r, t; r_0, t)r_0dr_0r dr - \frac{4i\rho_0\omega\overline{U}_2(x = t)}{r_1^2(r_2^2 - r_1^2)} \int_0^{r_1} \int_{r_1}^{r_2} G_2(r, t; r_0, t)r_0dr_0r dr, \quad (\text{A25})$$

$$\overline{P}_2(x = t) = -\frac{4i\rho_0\omega\overline{U}_1(x = t)}{r_1^2(r_2^2 - r_1^2)} \int_{r_1}^{r_2} \int_0^{r_1} G_2(r, t; r_0, t)r_0dr_0r dr - \frac{4i\rho_0\omega\overline{U}_2(x = t)}{(r_2^2 - r_1^2)^2} \int_{r_1}^{r_2} \int_{r_1}^{r_2} G_2(r, t; r_0, t)r_0dr_0r dr. \quad (\text{A26})$$

The resultant Eqs. (A23)–(A26) in addition to the tensor Eqs. (A15) and (A16) provide a solvable system of eight equations from which averaged pressure and velocity terms defined in Eqs. (A1)–(A8) as eight variables may readily be calculated. Please note that, in the calculation of the numerical integrals present in Eqs. (A23)–(A26), a sufficient number of the summations [n in Eqs. (A18) and (A19)] needs to be considered in order to yield accurate results. Herein, a sufficient number of summations has been considered to ensure that the relative difference between the resultant partial summation and the exact summation value does not exceed 1%.

Followed by the derivation of the averaged pressure and velocity discussed herein, the overall pressure and velocity field on the two sides of the transverse bilayer metamaterial may be written as

$$P(x = 0) = \frac{1}{\pi r_2^2} [\pi r_1^2 \overline{P}_1(x = 0) + \pi (r_2^2 - r_1^2) \overline{P}_2(x = 0)], \quad (\text{A27})$$

$$P(x = t) = \frac{1}{\pi r_2^2} [\pi r_1^2 \overline{P}_1(x = t) + \pi (r_2^2 - r_1^2) \overline{P}_2(x = t)], \quad (\text{A28})$$

$$u(x = 0) = \frac{1}{\pi r_2^2} [\overline{U}_1(x = 0) + \overline{U}_2(x = 0)], \quad (\text{A29})$$

$$u(x = t) = \frac{1}{\pi r_2^2} [\overline{U}_1(x = t) + \overline{U}_2(x = t)]. \quad (\text{A30})$$

Eventually, utilizing Eqs. (A27)–(A30), the transfer matrix that corresponds to the transverse bilayer metamaterial may be constructed as follows:

$$\begin{bmatrix} P(x = 0) \\ u(x = 0) \end{bmatrix} = \begin{bmatrix} M_{11} & M_{12} \\ M_{21} & M_{22} \end{bmatrix} \begin{bmatrix} P(x = t) \\ u(x = t) \end{bmatrix} \quad (\text{A31})$$

From which the transmittance may be readily calculated as [33]

$$T = \left| \frac{2}{M_{11} + M_{12}/\rho_0c_0 + M_{21}\rho_0c_0 + M_{22}} \right|^2. \quad (\text{A32})$$

APPENDIX B: METHODS

1. Numerical simulation

All simulations were performed with COMSOL MULTI-PHYSICS finite element software using the pressure-acoustic module in the frequency domain. The waveguide and UOM structures are considered as perfectly rigid media, and the perfectly matched layer has been implemented to enclose the computational domain to mitigate subsequent reflections.

2. Metamaterial fabrication

A UOM structure with dimensions of $t = 5.2$, $r_1 = 5.1$, $r_2 = 7$ cm, and $\phi = 8.2^\circ$ was fabricated using a commercial 3D printer (Dimension SST 1200es) from ABS plastic with a resolution of 0.2 mm. Next, the fabricated UOM was postprocessed using a two-part epoxy resin (BJB Enterprise TC-1614 A/B) that sealed the internal porous nature of the 3D printed UOM thereby providing improved mechanical properties.

3. Experimental setup and procedure

The transmittance through the UOM was experimentally obtained using an in-house built impedance tube. The impedance tube setup was designed and fabricated in accordance with the American Society for Testing and Materials (ASTM) E 2611-09 standard [34]. The setup featured a speaker enclosed in a soundproof box that predominately guided the acoustic wave towards the impedance tube and eliminated the effect of back reflections from the experimental environment. The impedance tube was composed of two schedule-40 PVC tubes with nominal diameters of 15.24 cm and a length of 1.5 m that were placed on either side of the UOM structure. In order to obtain the transmittance through the UOM, the transfer matrix of the UOM was retrieved for two different types of terminations as discussed in ASTM E 2611-09 and, by sweeping the loudspeaker's input frequency, the transmittance was obtained across the frequency range of 300–600 Hz. Noteworthy, experimental transmittance herein has been obtained by employing the two-load method in which open-end and semianechoic terminations were utilized.

- [1] A. Selamet and Z. L. Ji, *J. Sound Vib.* **223**, 197 (1999).
- [2] L. Huang, *J. Acoust. Soc. Am.* **119**, 2628 (2006).
- [3] C. Wang, L. Cheng, and L. Huang, *J. Sound Vib.* **318**, 792 (2008).
- [4] J. W. Lee and G.-W. Jang, *Int. J. Numer. Methods Eng.* **91**, 552 (2012).
- [5] N. Sellen, M. Cuesta, and M. Galland, *J. Sound Vib.* **297**, 492 (2006).
- [6] G. W. Stewart, *Phys. Rev.* **31**, 696 (1928).
- [7] Y. Xie, W. Wang, H. Chen, A. Konneker, B.-I. Popa, and S. A. Cummer, *Nat. Commun.* **5**, 5553 (2014).
- [8] R. Ghaffarivardavagh, J. Nikolajczyk, R. Glynn Holt, S. Anderson, and X. Zhang, *Nat. Commun.* **9**, 1349 (2018).
- [9] Y. Li, X. Jiang, R.-q. Li, B. Liang, X.-y. Zou, L.-l. Yin, and J.-c. Cheng, *Phys. Rev. Appl.* **2**, 064002 (2014).
- [10] J. Zhu, J. Christensen, J. Jung, L. Martin Moreno, X. Yin, L. Fok, X. Zhang, and F. J. Garcia Vidal, *Nat. Phys.* **7**, 52 (2010).
- [11] D. Lu and Z. Liu, *Nat. Commun.* **3**, 1205 (2012).
- [12] H. Chen and C. T. Chan, *Appl. Phys. Lett.* **91**, 183518 (2007).
- [13] S. A. Cummer, B.-I. Popa, D. Schurig, D. R. Smith, J. Pendry, M. Rahm, and A. Starr, *Phys. Rev. Lett.* **100**, 024301 (2008).
- [14] J. W. Jung, J. E. Kim, and J. W. Lee, *Appl. Phys. Lett.* **112**, 041903 (2018).
- [15] C. Shen, Y. Xie, J. Li, S. A. Cummer, and Y. Jing, *J. Appl. Phys.* **123**, 124501 (2018).
- [16] X. Wu, K. Y. Au-Yeung, X. Li, R. C. Roberts, J. Tian, C. Hu, Y. Huang, S. Wang, Z. Yang, and W. Wen, *Appl. Phys. Lett.* **112**, 103505 (2018).
- [17] S. H. Kim and S. H. Lee, *AIP. Adv.* **4**, 117123 (2014).
- [18] G. Ma, M. Yang, Z. Yang, and P. Sheng, *Appl. Phys. Lett.* **103**, 011903 (2013).
- [19] Z. Chen, L. Fan, S.-y. Zhang, H. Zhang, X.-j. Li, and J. Ding, *Appl. Phys. Express* **8**, 107301 (2015).
- [20] V. M. García-Chocano, S. Cabrera, and J. Sánchez-Dehesa, *Appl. Phys. Lett.* **101**, 184101 (2012).
- [21] L.-j. Li, B. Zheng, L.-m. Zhong, J. Yang, B. Liang, and J.-c. Cheng, *Appl. Phys. Lett.* **113**, 103501 (2018).
- [22] G. C. Lauchle, J. R. MacGillivray, and D. C. Swanson, *J. Acoust. Soc. Am.* **101**, 341 (1997).
- [23] Y. Niu and Y. J. Kim, *Noise Control. Eng. J.* **60**, 392 (2012).
- [24] R. Alfredson and P. Davies, *J. Sound Vib.* **13**, 389 (1970).
- [25] U. Fano, *Phys. Rev.* **124**, 1866 (1961).
- [26] A. Fellay, F. Gagel, K. Maschke, A. Virlouvet, and A. Khater, *Phys. Rev. B* **55**, 1707 (1997).
- [27] C. Goffaux, J. Sánchez-Dehesa, A. L. Yeyati, P. Lambin, A. Khelif, J. O. Vasseur, and B. Djafari-Rouhani, *Phys. Rev. Lett.* **88**, 225502 (2002).
- [28] R. Sainidou and N. Stefanou, *Phys. Rev. B* **73**, 184301 (2006).
- [29] Q. Feng, Z. Huang, G. Yu, and X. Meng, *J. Acoust. Soc. Am.* **134**, EL345 (2013).
- [30] Y. Li, G. Yu, B. Liang, X. Zou, G. Li, S. Cheng, and J. Cheng, *Sci. Rep.* **4**, 6830 (2014).
- [31] X. Zhu, K. Li, P. Zhang, J. Zhu, J. Zhang, C. Tian, and S. Liu, *Nat. Commun.* **7**, 11731 (2016).
- [32] H. Esfahlani, H. Lissek, and J. R. Mosig, *Phys. Rev. B* **95**, 024312 (2017).
- [33] I. L. Vér and L. L. Beranek, *Noise and Vibration Control Engineering: Principles and Applications* (Wiley, Hoboken, NJ, 1992).
- [34] *ASTM E2611-09, Standard Test Method for Measurement of Normal Incidence Sound Transmission of Acoustical Materials Based on the Transfer Matrix Method* (ASTM International, West Conshohocken, PA, 2009).